Acoustic Asymptotic Inversion and AVO

Kidane Araya and William W. Symes

ABSTRACT

Prestack asymptotic linearized acoustic inversion, like other forms of prestack depth migration, produces image volumes exhibiting amplitude-versus-offset variation which may be indicative of hydrocarbon accumulations. A careful analysis a seismic line from the offshore Gulf of Mexico suggests that the prestack acoustic inversion volume may be more consistent with the physics underlying AVO analysis than are other possible input data volumes, yielding more consistent predictions of gradient and intercept across a wider range of angles.

INTORDUCTION

According to (Shuey, 1985), the compressional wave reflection coefficient can be approximated by a linear function of the form,

$$R_{pp}(\theta) \simeq I + G \sin^2 \theta \tag{1}$$

where θ is the angle of incidence, and this approximation should be accurate for roughly $\theta \leq 30^o$ and for modest contrasts in material properties. I, the intercept or normal incidence reflection coefficient, is proportional to the local fluctuation in acoustic impedance. The gradient G is an approximate measure of changes in Poisson's ratio. See (Foster et al., 1997) for a careful discussion of the scope of this approximation.

Given R_{pp} as a function of depth (or time) and midpoint, regression according to this model produces sections of I and G estimates. In many areas of the world the ratio G/I is roughly constant within a sedimentary column at depths inhabited by shales or brine-filled sands, so that a I-G crossplot is clustered along a "fluid line" (Smith and Gidlow, 1987). However the presence of hydrocarbons may cause a marked change in this ratio. Such "AVO anomalies" are a powerful exploration tool, indicative of lithology and pore fluid contents., see for instance (Rutherford and Williams, 1989).

Various prestack data volumes can stand in for of R_{pp} in estimation of G and I. The common choice, NMO-corrected CDP gathers, does not have a clear relation to the theory underlying the analysis of R_{pp}. Thus one might wonder whether a more wave-equation based processing sequence would produce data better suited in some way to AVO analysis. In particular, almost any data with coherence will fit a linear relation like Shuey's over a small range of angles. However extension of the relation to the full angular range ($0 \leq \theta \leq 30^o$) would produce estimates of I, G with more statistical power, but only if the data exhibits considerable consistency with the theory.

We have applied AVO analysis to a variety of prestack data volumes extracted from a marine seismic line from the Gulf of Mexico. The data show a very bright event, caused by a large and very productive gas sand, which exhibits pronounced anomalous AVO behaviour. The prestack data input to our analysis included NMO-corrected CDP gathers and several varieties of prestack depth migration. While all input data gave roughly similar results consistent with Shuey's relation and the known location of the gas reservoir over a narrow range of angles, only the prestack acoustic inversion volume exhibited a well-defined fluid line over the full angular range predicted by the theory.

We are certainly not the first to suggest the virtues of inversion as an AVO tool - see for example (Bourgeois et al., 1989; Pan et al., 1993; Foster et al., 1997). The results presented below may be yet another piece of evidence that (visco)elastic wave propagation is sometimes an adequate model for detailed analysis of reflected waves in the sedimentary crust.

Our analysis consisted of three stages, corresponding to the sections to follow: 1) preprocessing and velocity control; 2) prestack imaging using five processing methods; 3) application of the same AVO attribute extraction method to all five prestack data volumes, and comparison of results.

Except as otherwise noted, all data processing was carried out using the ProMAX™ 2D package marketed by Landmark Graphics.

DATA, PREPROCESSING, AND VELOCITY ANALYSIS

The data used in this study is part of a survey conducted in the Mississippi Canyon of the Gulf of Mexico by Exxon Production Research Company, which made the data available to The Rice Inversion Project for use in research in seismic inversion. Table (1) displays acquisition parameters for the survey.

Preprocessing of the data included: sorting to CDP gathers, estimation of the source wavelet from the CDP, removal of the source signature and infill of missing traces, zero-phase bandpass filter with 75 Hz high cut, velocity analysis, NMO, stack Figure (1), and poststack phase shift migration Figure (2).

In the study area, the region above 1 s two-way time is quite structured, with features resembling buried paleochannels and small throw faults, as is evident in the CDP stack Figure (1). However below roughly 1.3 - 1.4 s the stack strongly suggests a nearly plane-layered structure. The prospective horizon, which is the very bright event at about 2.3 s, is embedded in more than a second of very flat-lying strata. Therefore it seemed likely that a laterally homogeneous velocity field would correctly account for the data kinematics. We produced a depth dependent interval velocity field using standard interactive velocity analysis technology. At the same CDP location, interval velocities obtained by automatic Differential Semblance velocity inversion in $p-\tau$ domain, Minkoff (1995) and Minkoff and

Air gun source	2000 PSI
Length of line	11182.5m
Number of shots	498
Number of receiver per shot	301
Shot interval	22.5m
Receiver interval	15m
Near offset	148m
Far offset	4648m
Source depth	5m
Cable depth	6m
Sampling rate	2ms
Trace length	5s

Table 1. Acquisition parameters for data used in this study.

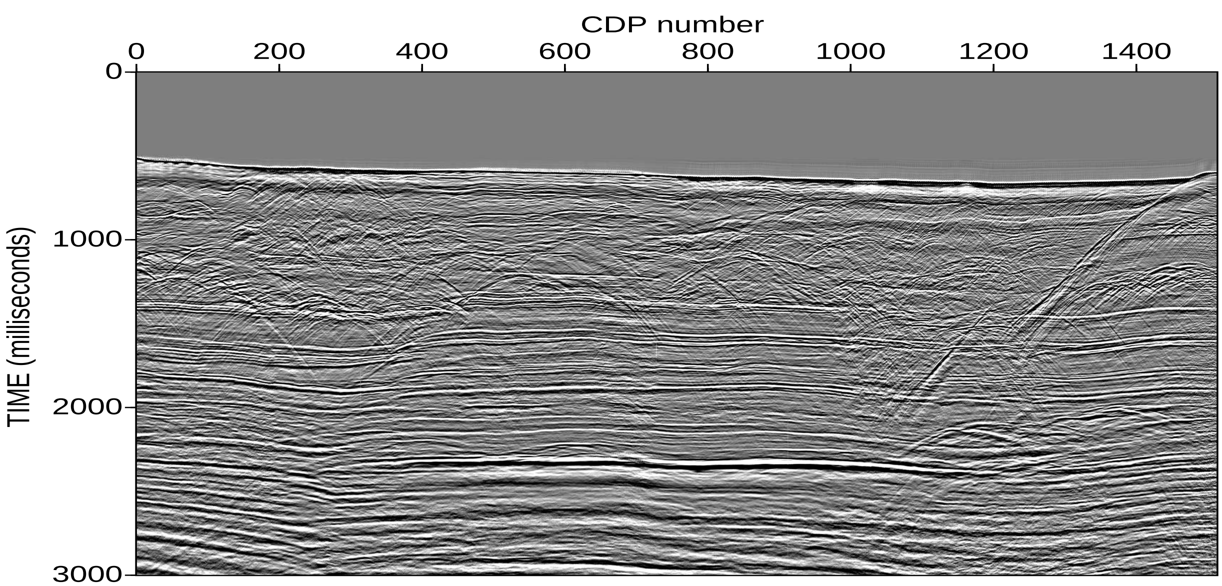

FIG. 1. CDP stack. The bright spot around 2300 msec in the middle of the section is the prospective horizon.

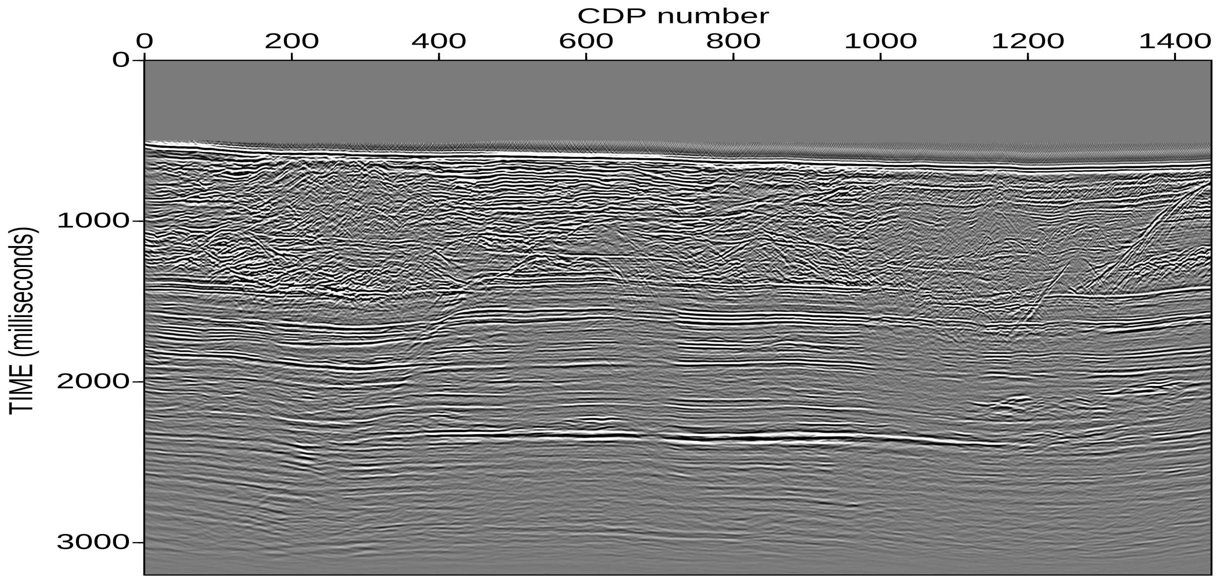

FIG. 2. Phase shift migration of the stacked data in Figure (1).

Symes (1997), were also available to us.

These two velocity profiles, obtained by very different methods, are in good agreement to the depth of the gas sand (~ 2.1 km, see Figure (3)). We verified the agreement by examining both prestack Common Image Gathers (CIGs) and postmigration stacks for several migration methods, using both velocity profiles. In all cases the results were visually equivalent and equally satisfactory. Therefore for the rest of this work we have used the velocity profile produced by inversion, which is the thicker line in Figure (3).

PRODUCTION OF PRESTACK IMAGE VOLUMES

We produced prestack data for input to AVO analysis by five methods:

1. NMO correction of CDP gathers
2. prestack Kirchhoff depth migration, without amplitude control
3. prestack Kirchhoff depth migration of data corrected for spherical divergence
4. prestack Kirchhoff depth migration with ray-based amplitude correction (sometimes called "true amplitude migration")
5. prestack asymptotic inversion for acoustic impedance

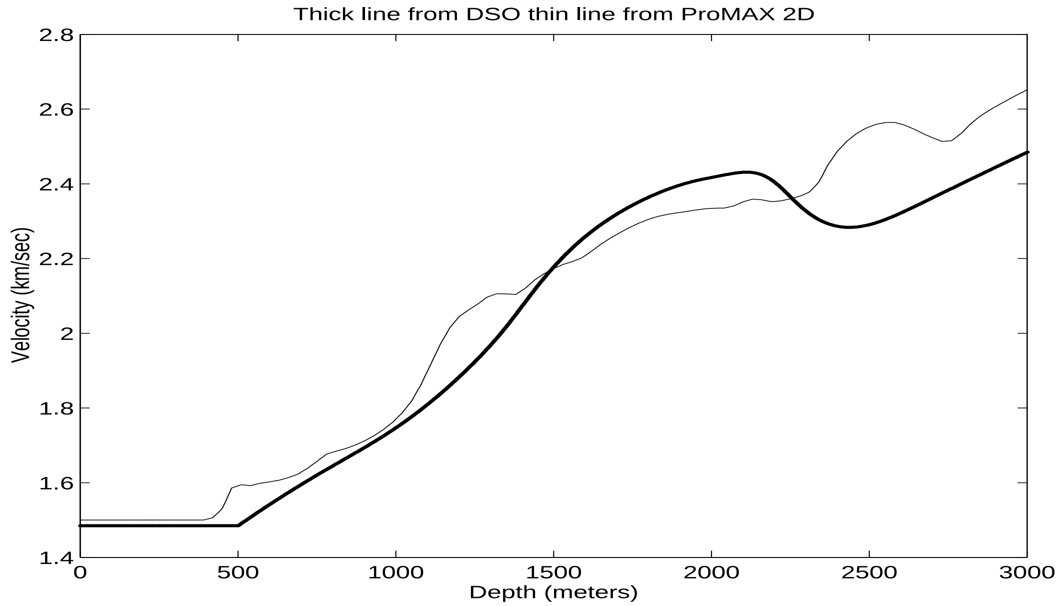

FIG. 3. Interval velocities from DSO (thick line) and interactive (thin line) velocity analysis.

The prestack inversion method (option 5) used here computes the traveltimes and amplitude factors using upwind finite difference schemes, as reported in (Symes et al., 1995a; Symes et al., 1995b; Araya and Symes, 1996). It accurately inverts the linearized acoustic forward model, which in turn accurately approximates the solution of the linearized acoustic wave equation. The computation of traveltimes and amplitudes used in this method incorporates an aperture limit. In the work reported here, only times at points connected to the source by rays lying within a 75^o aperture were computed accurately; reflections involving more steeply dipping rays were automatically suppressed.

Methods 2 - 5 accept common offset gathers, and produce depth dependent volumes. We used a depth-to-time conversion to prepare these data for input to the AVO estimation module, which expected time data.

In all cases we used offsets limited to 1918 m, since greater offsets produced rays with incidence angles greater than 30^o at the gas sand target, invalidating Shuey's approximate AVO relation. Thus in all cases we migrated/inverted 119 different offsets ranging from 148m to 1918m, for 498 shot positions. The sample interval in depth was in all cases 4 m.

We compared and quality controlled the five variants of prestack imaging listed above in two ways: 1) examination of Common Image gathers, which should show only flat events if the velocity analysis has been successful; 2) production of stacked images. Since AVO estimation is notoriously sensitive to velocity errors (Spratt, 1987), this type of control is very important. In all cases CIG gathers below 1.4 s were quite flat, and no residual moveout correction seemed necessary. Here we show only the post-migration (or -NMO, or -inversion) stacked images. The CDP stack is shown in Figure (1), as already noted, along with its phase shift migration (Figure (2)). The prestack migration results appear as Figures (4), (5), (6), and (7), corresponding to options 2 - 5 in the list above

We observe that the post-migrations stacks of prestack migrated data are very similar in almost every detail. Although the velocity field used in all cases is only depth dependent, the prestack results all more clearly image and correctly position faults and other steeply dipping events than does the poststack time migration shown in Figure (2).

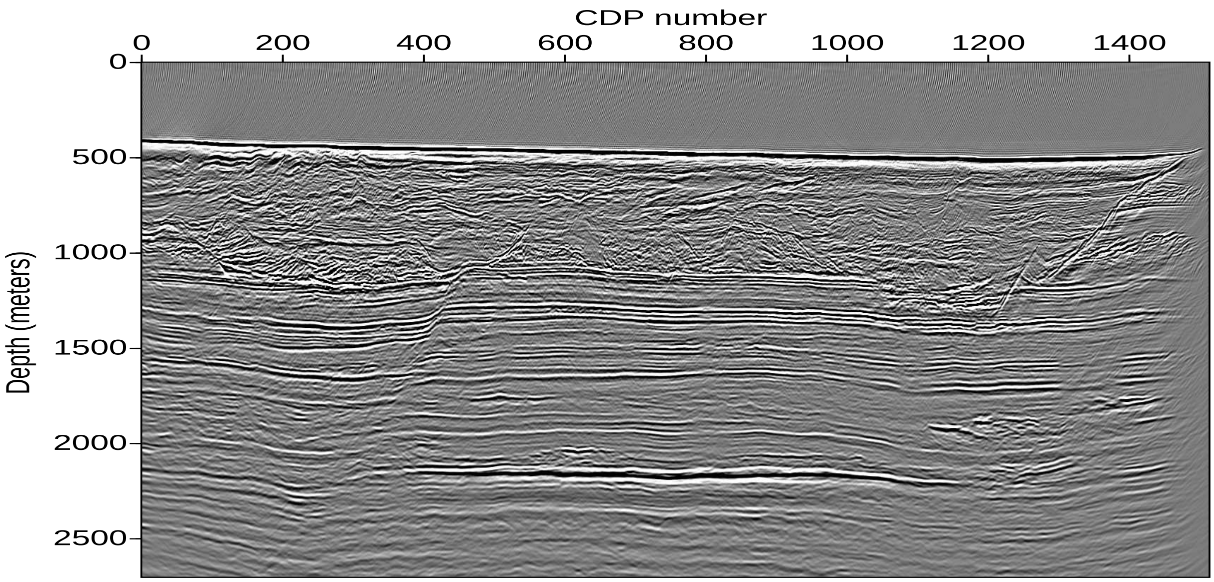

FIG. 4. Post migration stack of common-offset prestack Kirchhoff depth migration data volume. Traveltimes computed using an implicit eikonal solver. Straightforward diffraction stack with no attempt to compensate for amplitude variation.

AVO ANALYSIS

AVO analysis consisted of the following steps:

1. sort 119 depth images volumes from offsets ranging 148-1918m to Common Image Gathers (CIGs), each referring to a common surface location;
2. convert depth to time using same velocity profile used in migration, sample at 2 ms;
3. compute angle of incidence for each time and offset;
4. produce I and G estimates for each time sample by regression according to Shuey's model.

Steps 1 and 2 were unnecessary for input of type 1., i.e. NMO-corrected CDP gathers, of course.

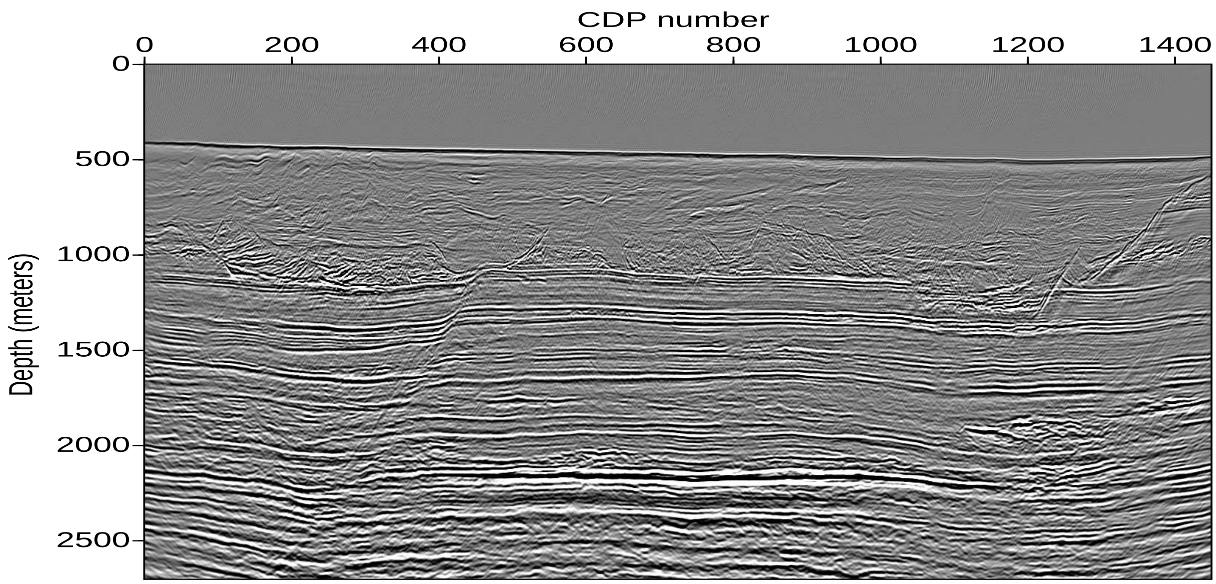

FIG. 5. Post migration stack of common-offset prestack Kirchhoff depth migration data volumen. Spherical spreading correction applied to data before migration. Traveltimes computed using an implicit eikonal solver.

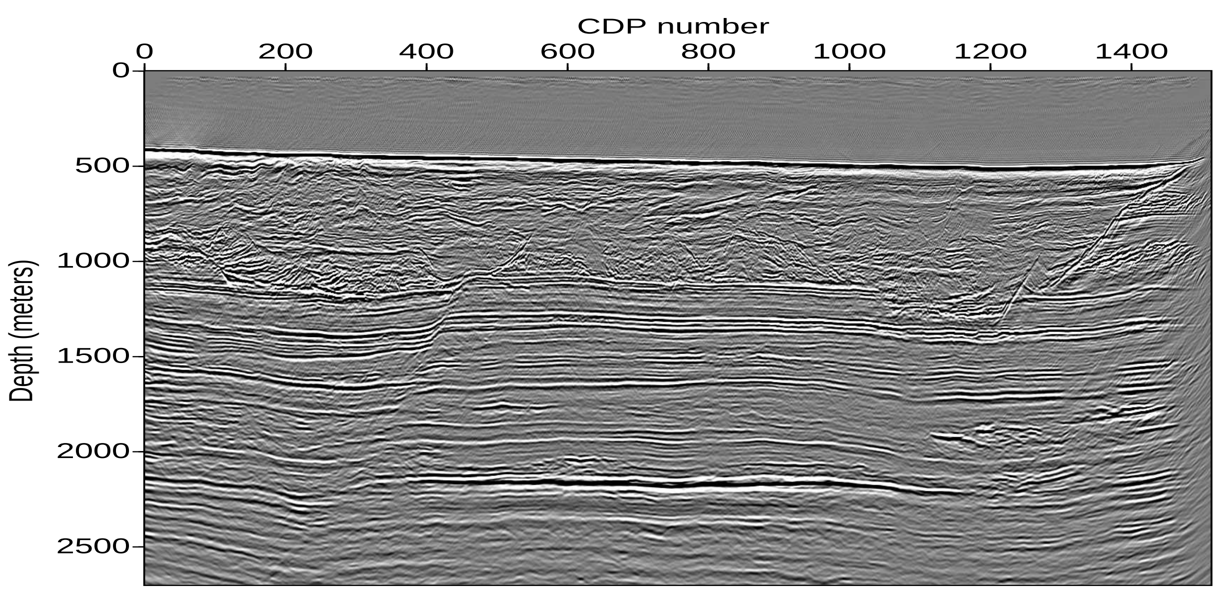

FIG. 6. Post inversion stack of common-offset prestack Kirchhoff "true amplitude" depth migration data volume. Traveltimes, spreading factor computed using ray tracer, amplitude correction applied during migration.

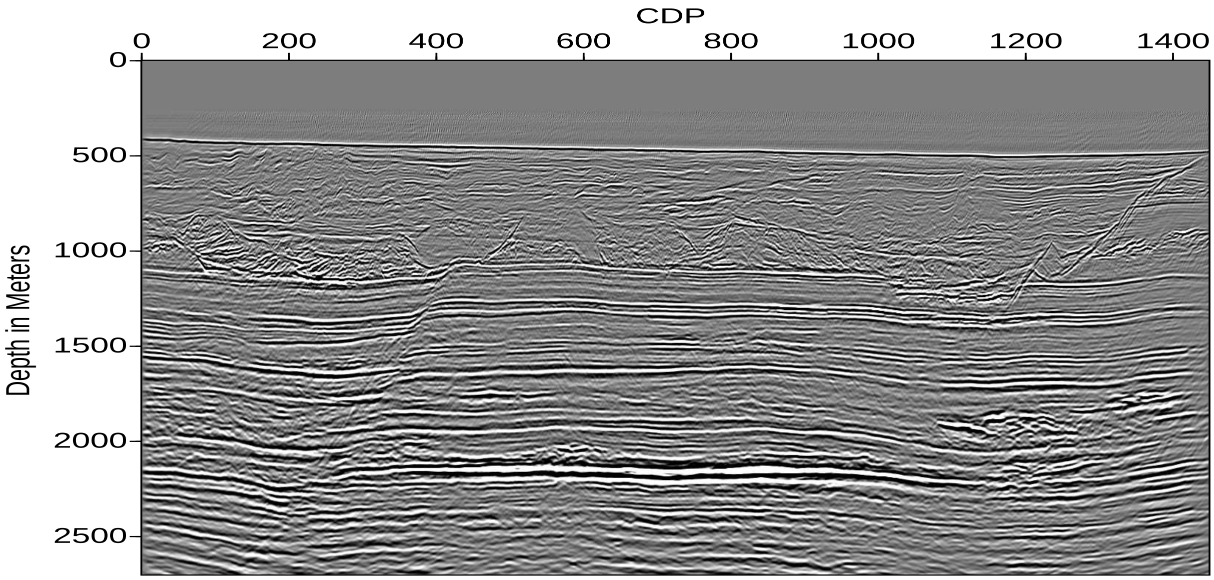

FIG. 7. Post inversion stack of asymptotic inversion data volume. Traveltimes and amplitude factors computed using upwind finite difference technique.

To explore the relation between consistency with Shuey's model, angle range, and type of input data, we produced I and G estimates for a single midpoint near the center of the gas sand using data from two angle of incidence ranges:

1. $5 - 10^o$, and

2. $5 - 30^o$.

We will refer to these as "narrow aperture" and "wide aperture" attribute estimates respectively.

For all ten experiments (two apertures, five input prestack data volumes for each) we have produced two displays:

1. crossplot of G versus I, with a theoretical fluid line superimposed;

2. distance from the fluid line for each I, G pair versus two way time

The theoretical fluid line is in our units $G = -I$, see for example (Foster et al., 1997) with allowances for units and the acoustic approximation (zero shear velocity). Note that in most cases it differs a little, in some cases a lot, from the line that would be obtain by regression on the computed I, G data.

We have differentiated the I, G pairs for the sedimentary column below the uncon-fomity (1400 - 2400 ms) from the pairs for the reservoir interval (2250 - 2350 ms) by plotting a plus sign on the former, a plus and a circle around the latter.

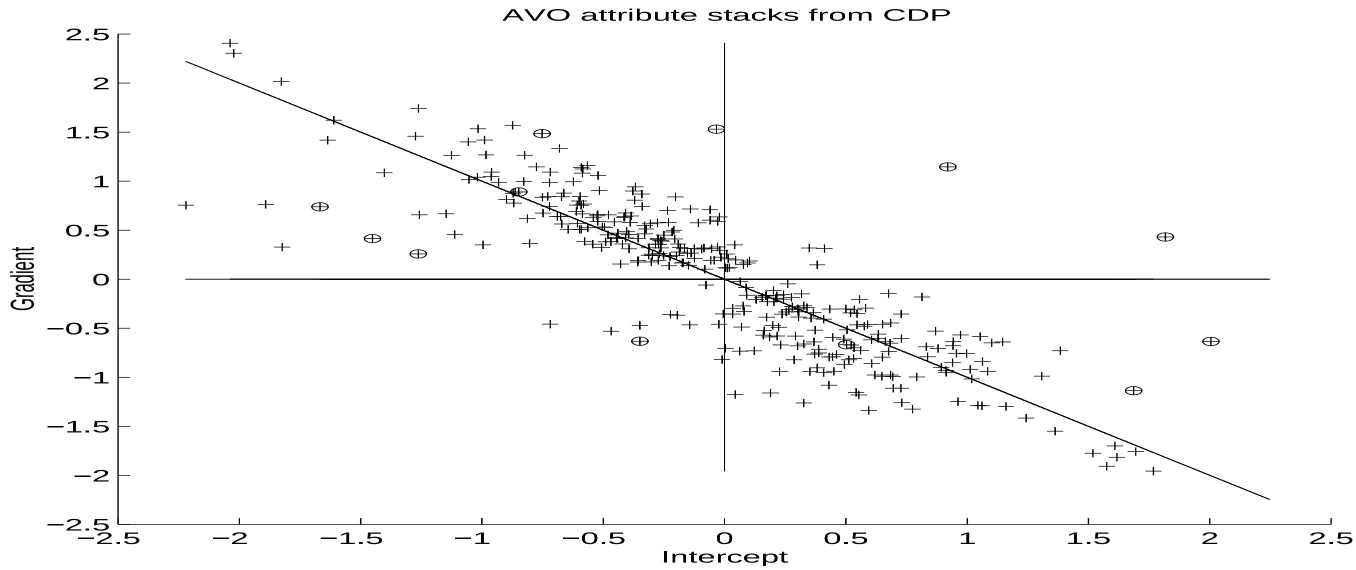

FIG. 8. Intercept versus gradient from CDP, narrow aperture.

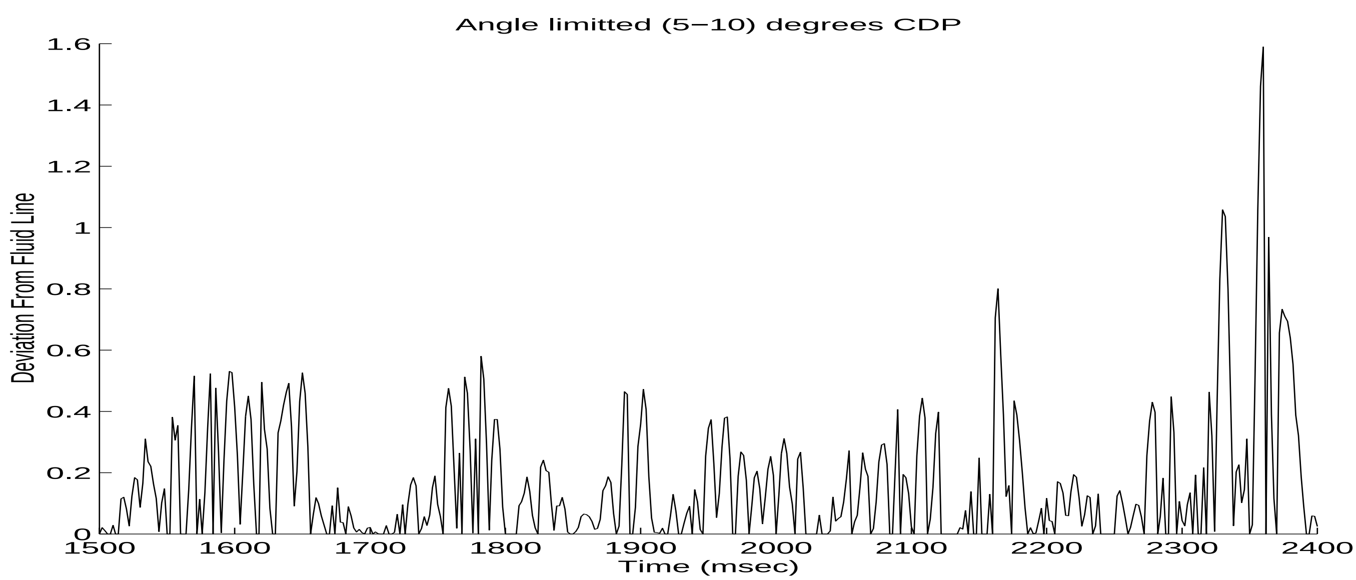

FIG. 9. Distance from fluid line for CDP, narrow aperture.

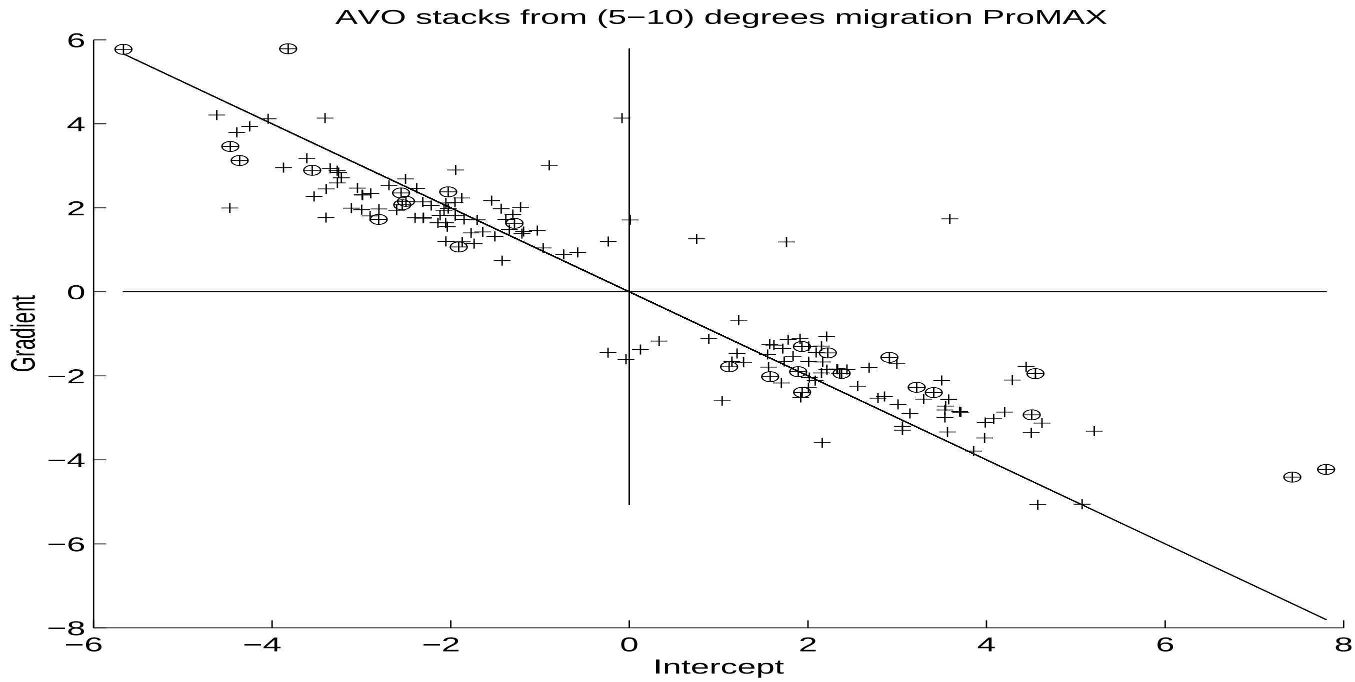

FIG. 10. Intercept versus gradient, CIG from common-offset prestack Kirchhoff migration (without amplitude processing), narrow aperture.

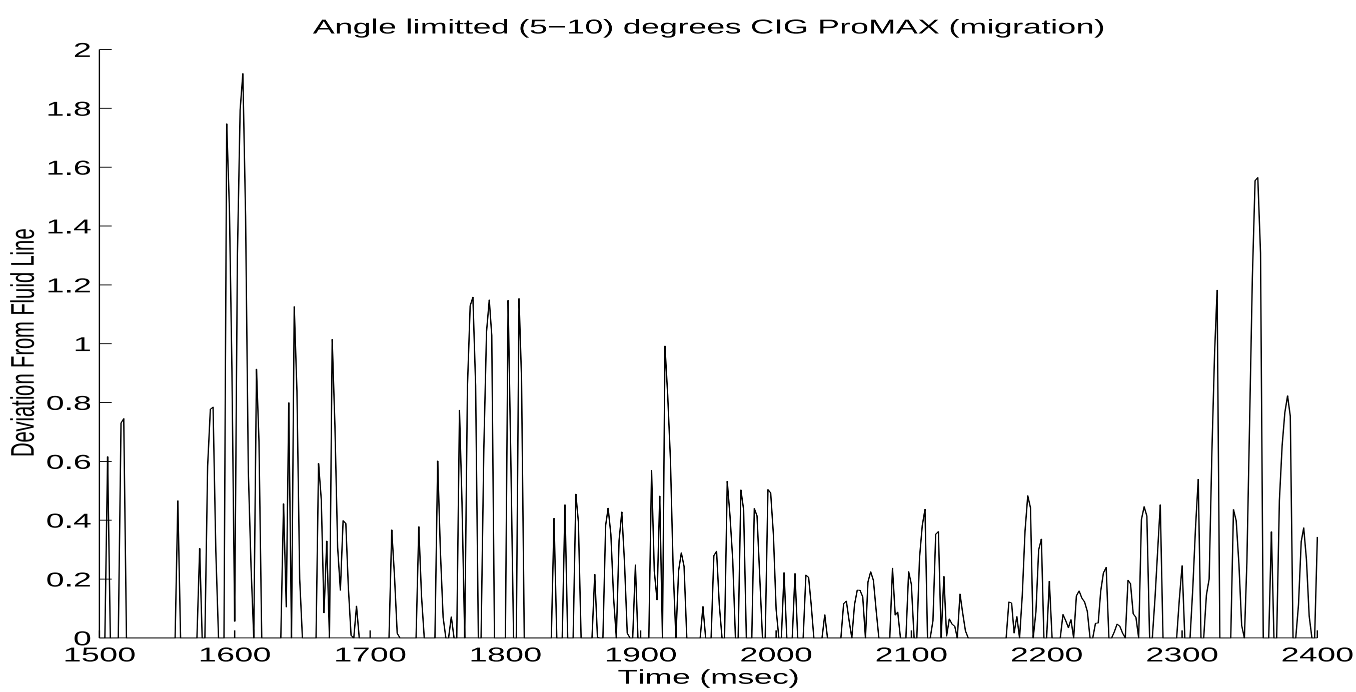

FIG. 11. Distance from fluid line, CIG from common-offset prestack Kirchhoff migration (without amplitude processing), narrow aperture.

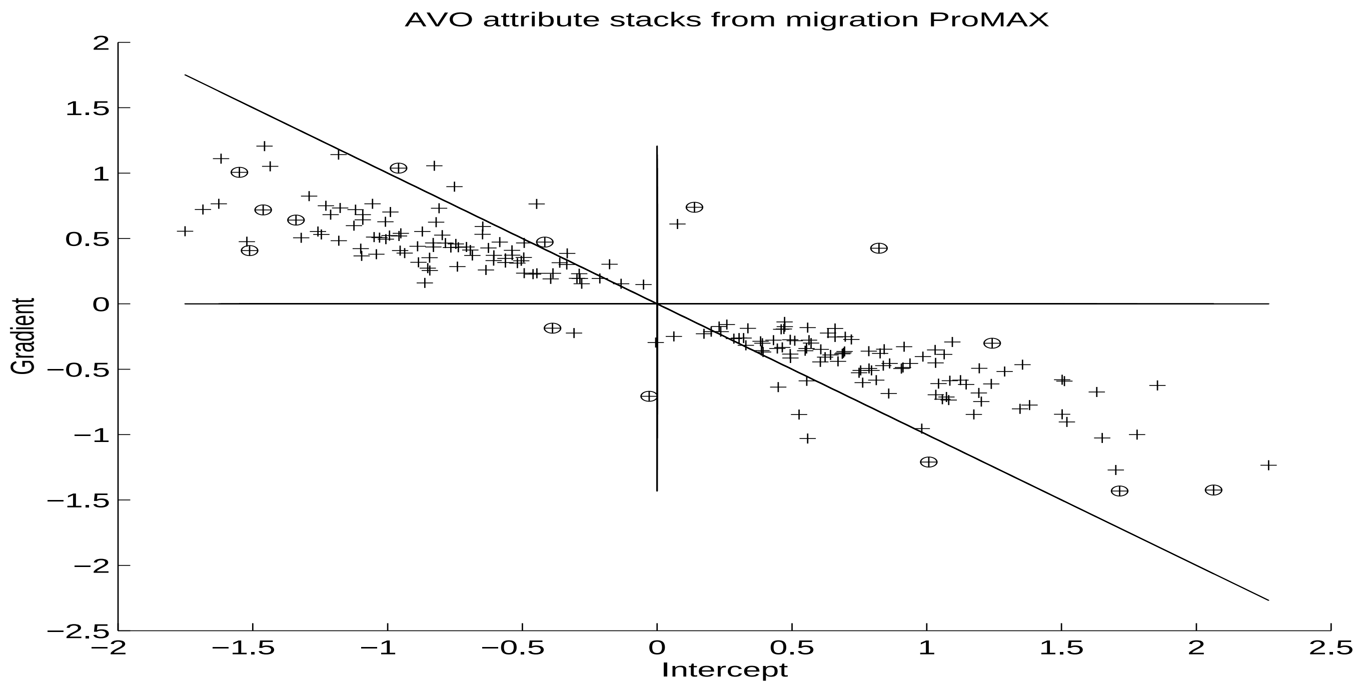

FIG. 12. Intercept versus gradient, CIG from common-offset prestack Kirchhoff migration, spherical spreading correction applied to data before migration, narrow aperture.

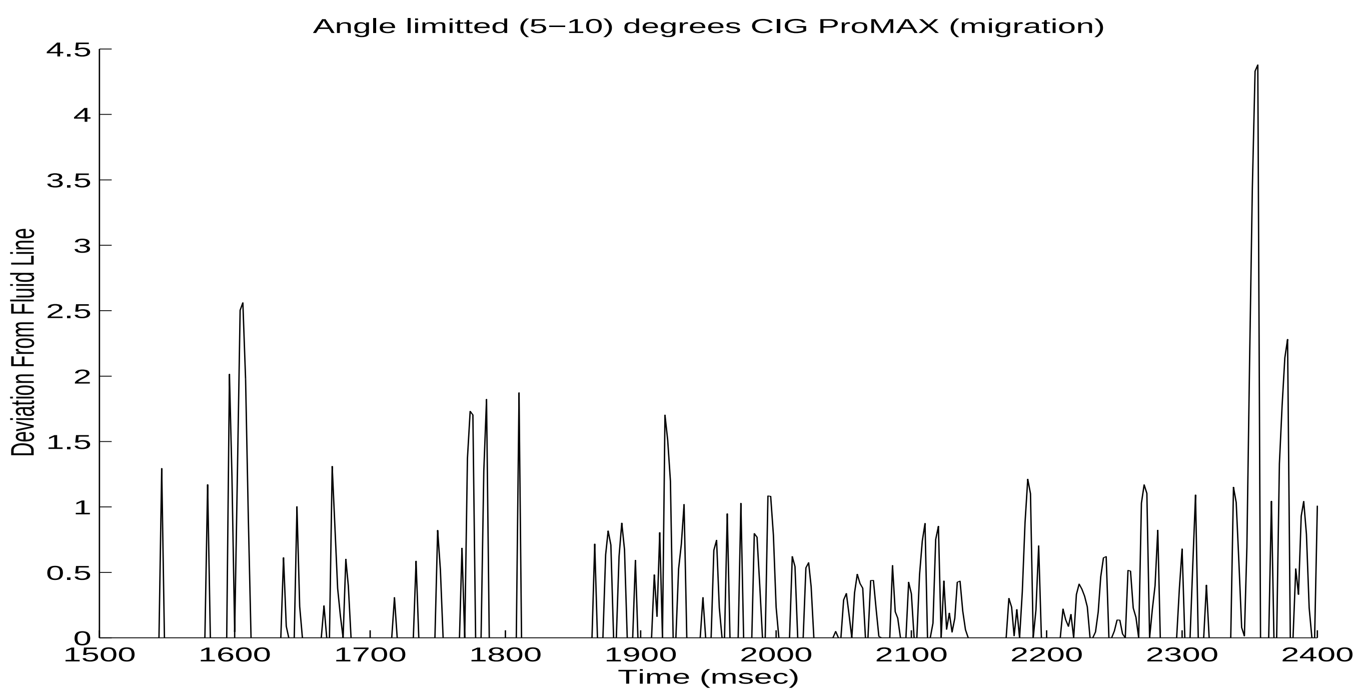

FIG. 13. Distance from fluid line, CIG from common-offset prestack Kirchhoff migration, spherical spreading correction applied to data before migration, narrow aperture.

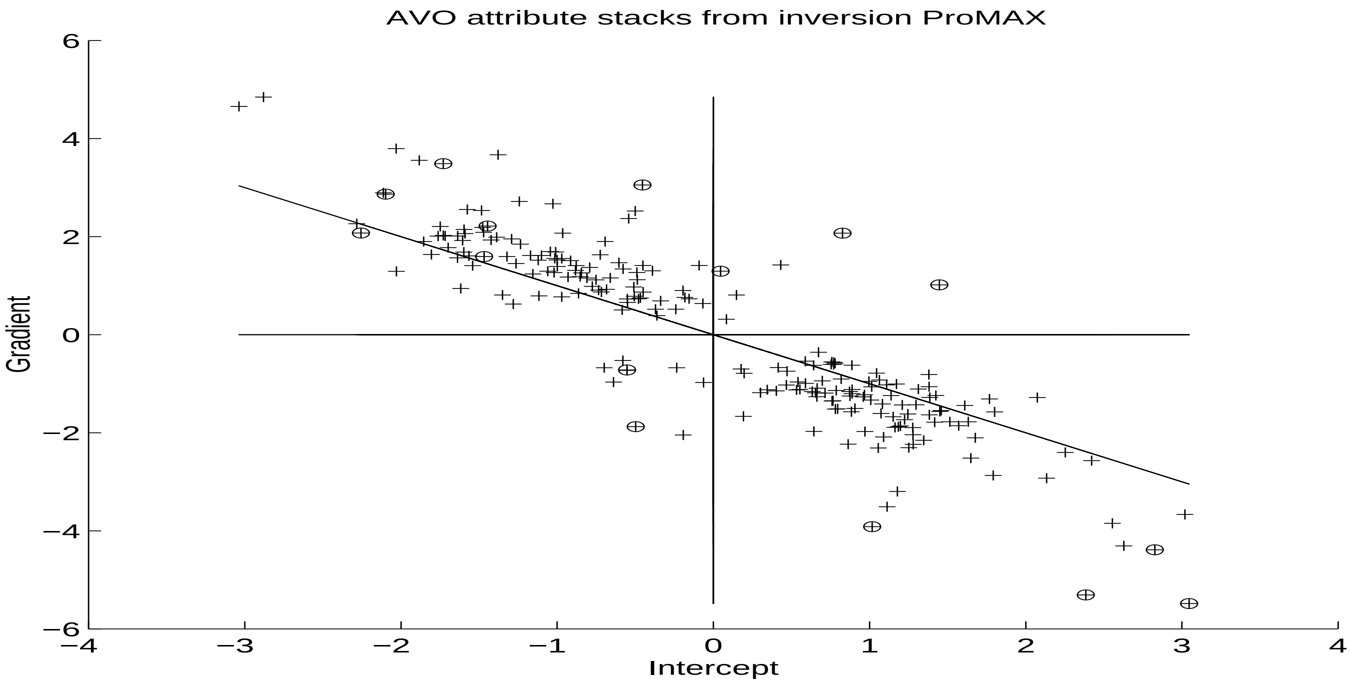

FIG. 14. Intercept versus gradient, CIG from common-offset prestack Kirchhoff true amplitude migration, narrow aperture.

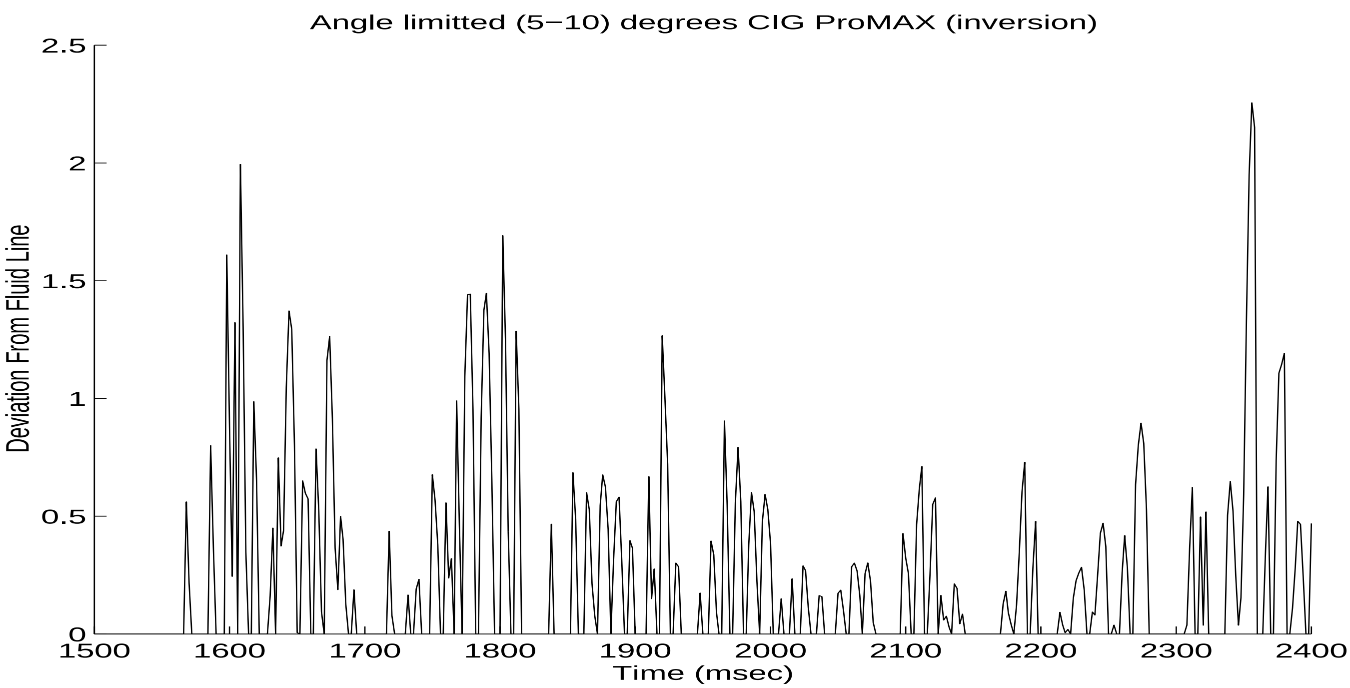

FIG. 15. Distance from fluid line, CIG from common-offset prestack Kirchhoff true amplitude migration, narrow aperture.

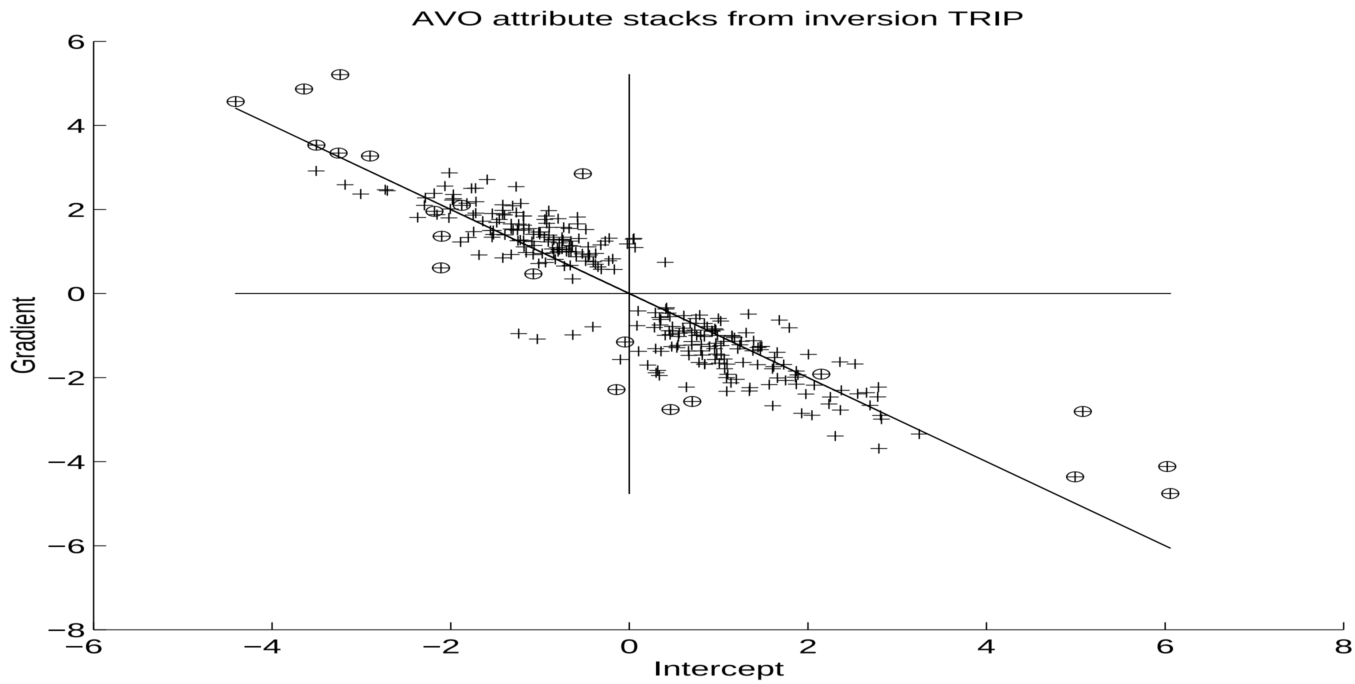

FIG. 16. Intercept versus gradient, CIG from asymptotic inversion, narrow aperture.

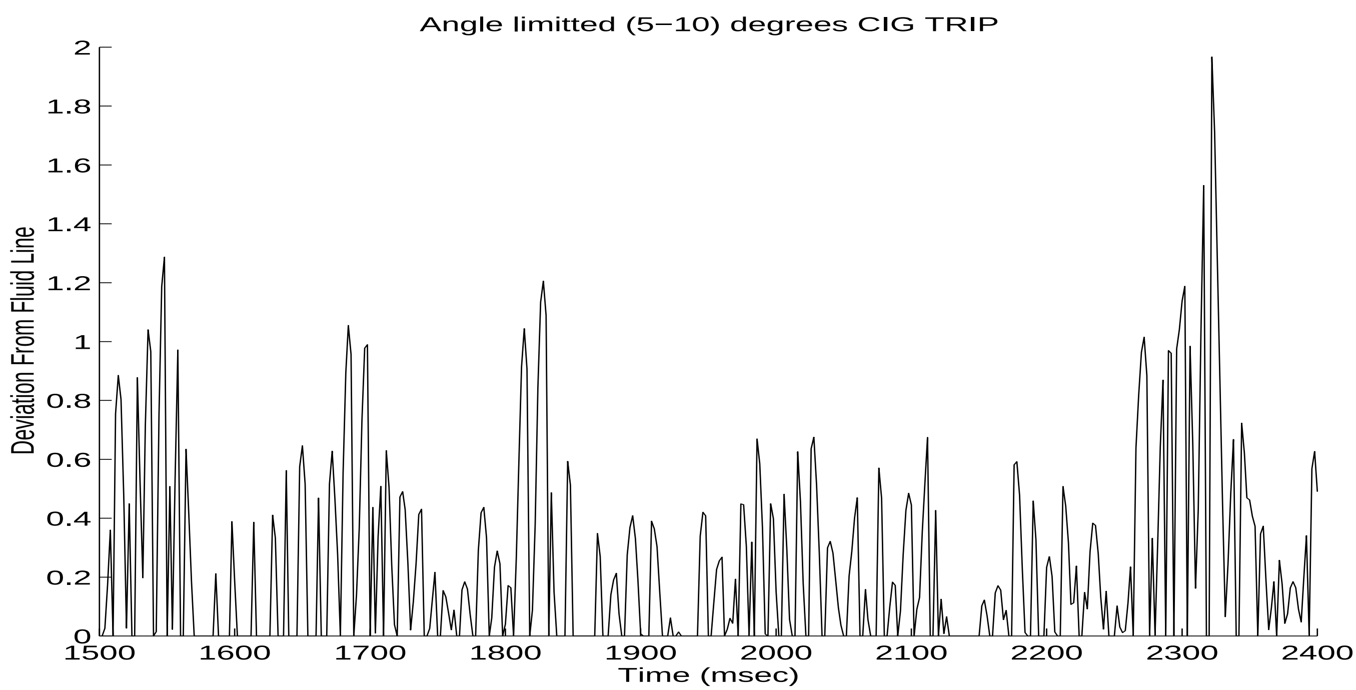

FIG. 17. Distance from fluid line, CIG from asymptotic inversion, narrow aperture.

The narrow angle results (Figures (8) through (17)) show clear clustering around the theoretical fluid line or something close to it. The Distance plot shows a clear distinction between the reservoir interval and the rest of the column in several cases (NMO-corrected CDP and asymptotic inversion). There are also suggestions of anomalies in several other zones, although these predictions are not consistent amongst the various input data types.

The wide angle results (Figures (18) through (27)) show considerably more scattered crossplots, *except* for the asymptotic inversion result (Figures (26), (27)), which remains clustered near the theoretical fluid line. Moreover only the NMO-corrected CDP and asymptotic inversion results retain unambigous, and in fact improved, resolution of AVO anomaly locations. The CDP crossplots is very scattered, however, and we speculate that a statistical analysis would assign considerably more power to the asymptotic inversion result.

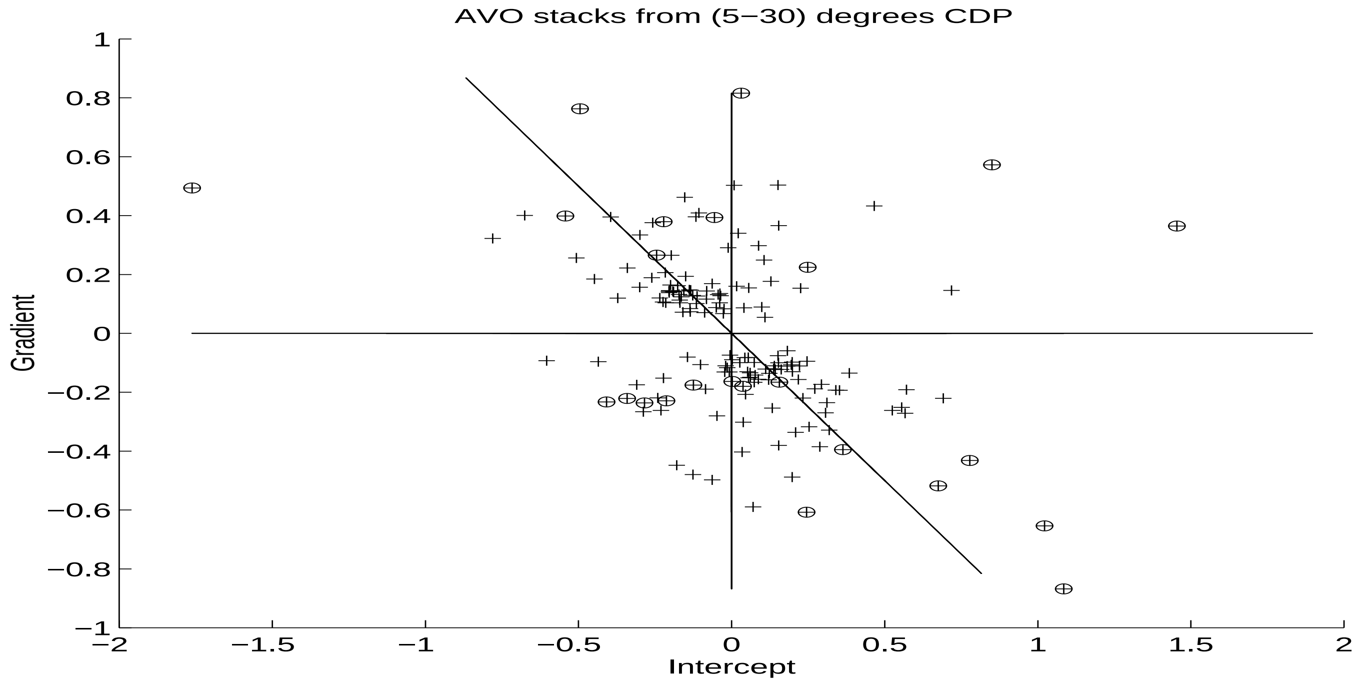

FIG. 18. Intercept versus gradient from CDP, wide aperture.

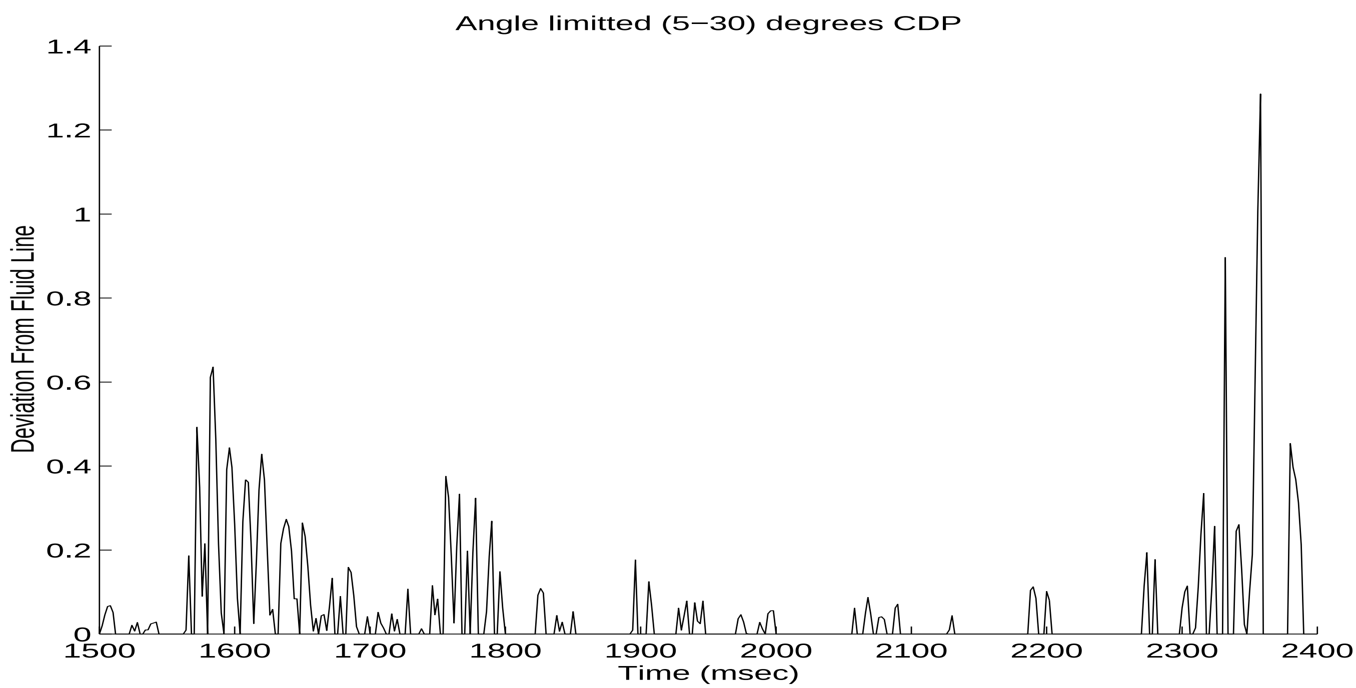

FIG. 19. Distance from fluid line for CDP, wide aperture.

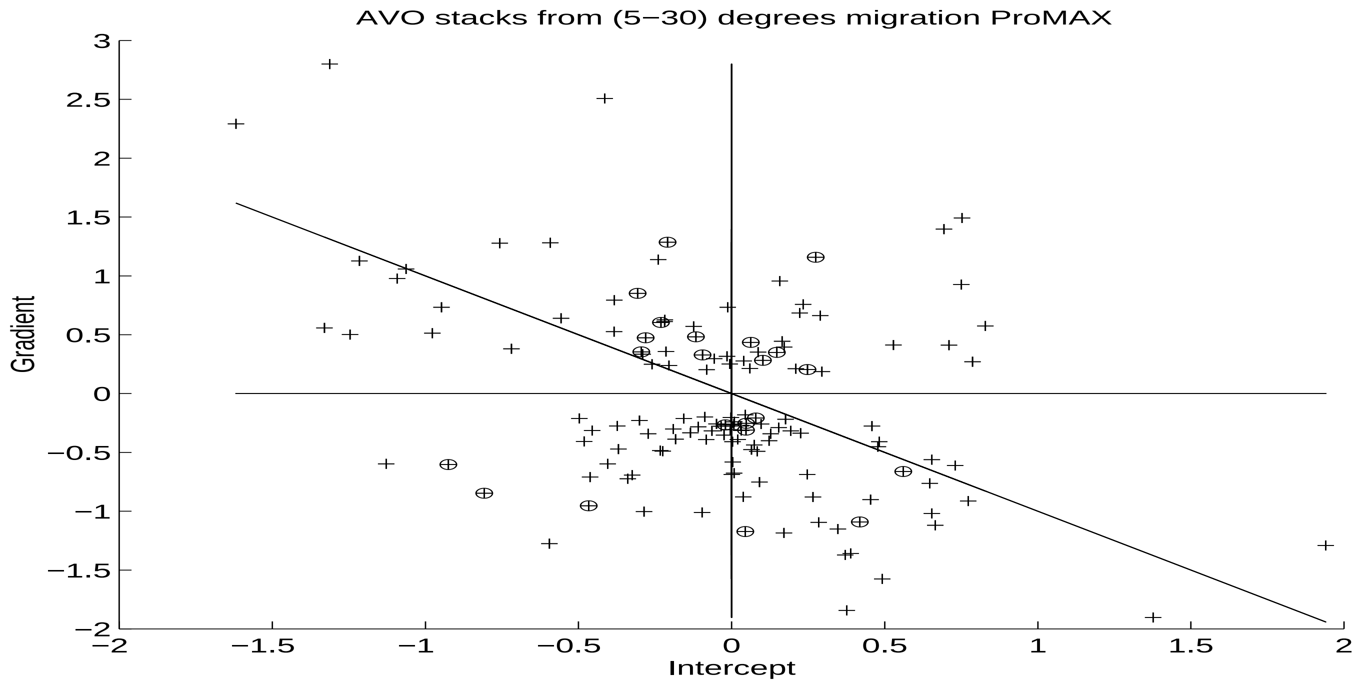

FIG. 20. Intercept versus gradient, CIG gathers from common-offset prestack Kirchhoff migration, no amplitude processing, wide aperture.

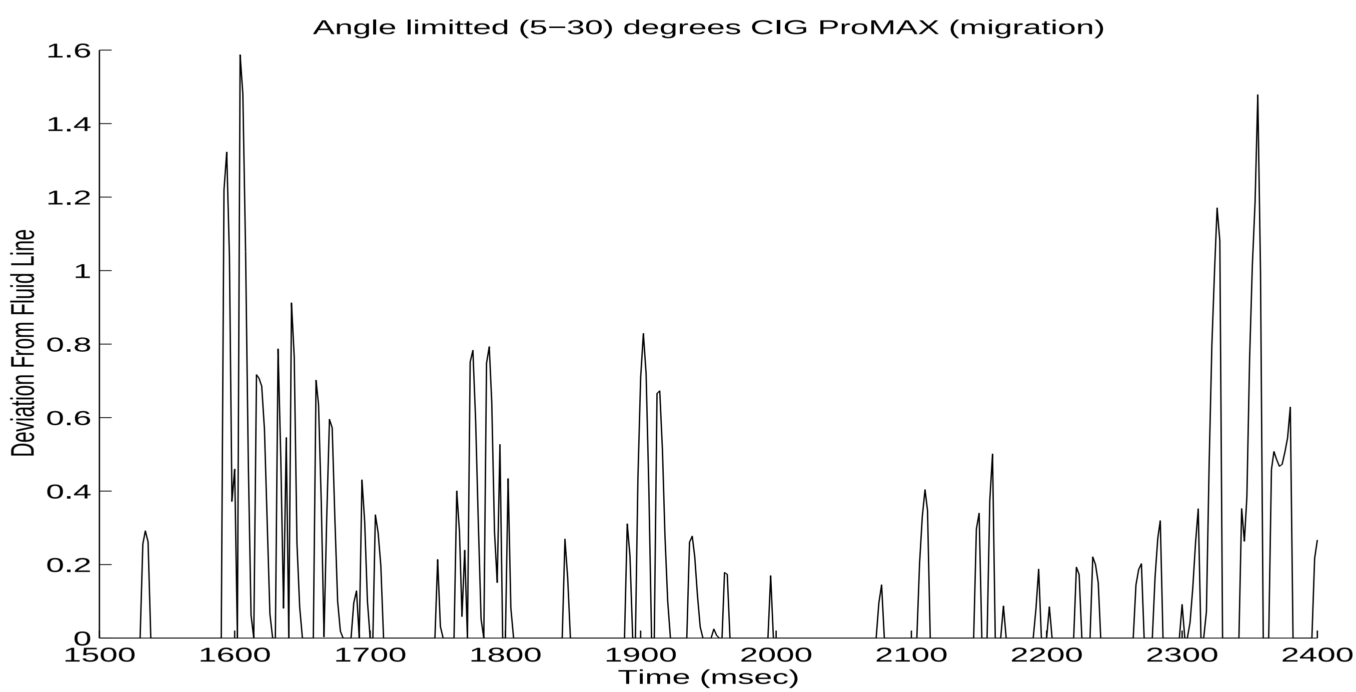

FIG. 21. Distance from fluid line, CIG from common-offset prestack Kirchhoff migration, no amplitude processing, wide aperture.

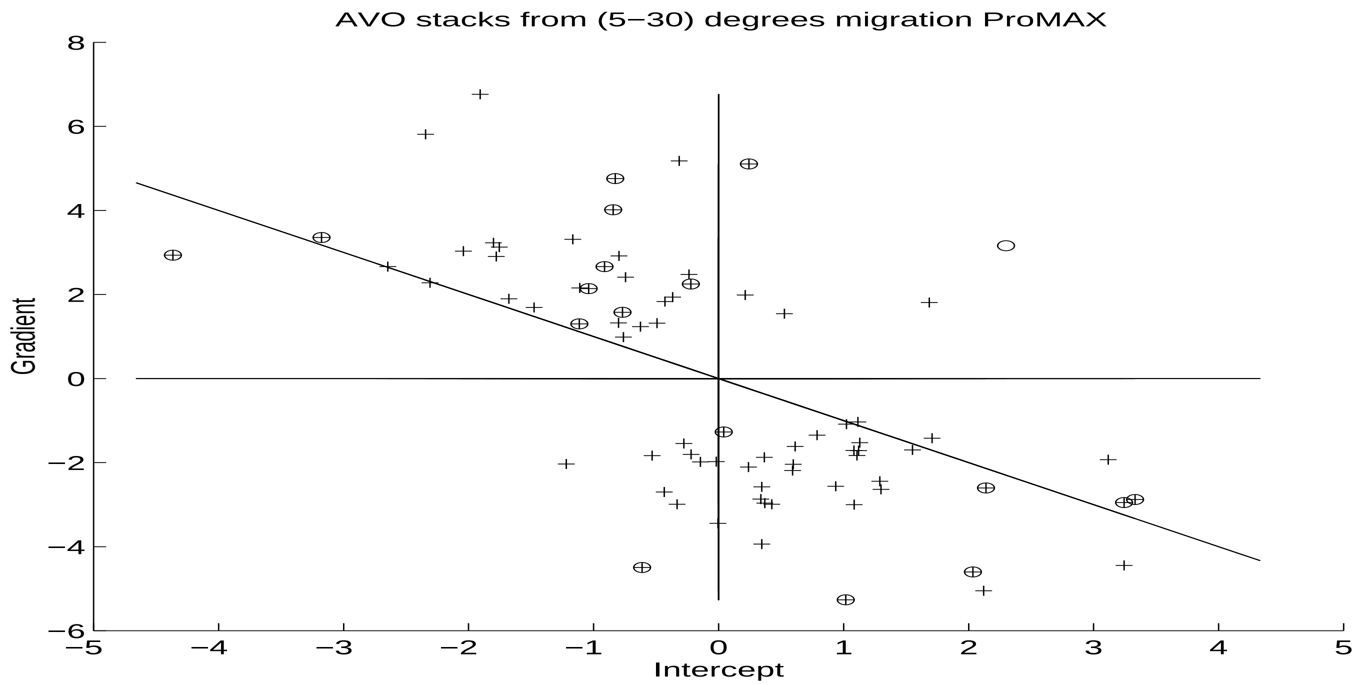

FIG. 22. Intercept versus gradient, CIG from common-offset prestack Kirchhoff migration, spherical spreading correction applied to data before migration, wide aperture.

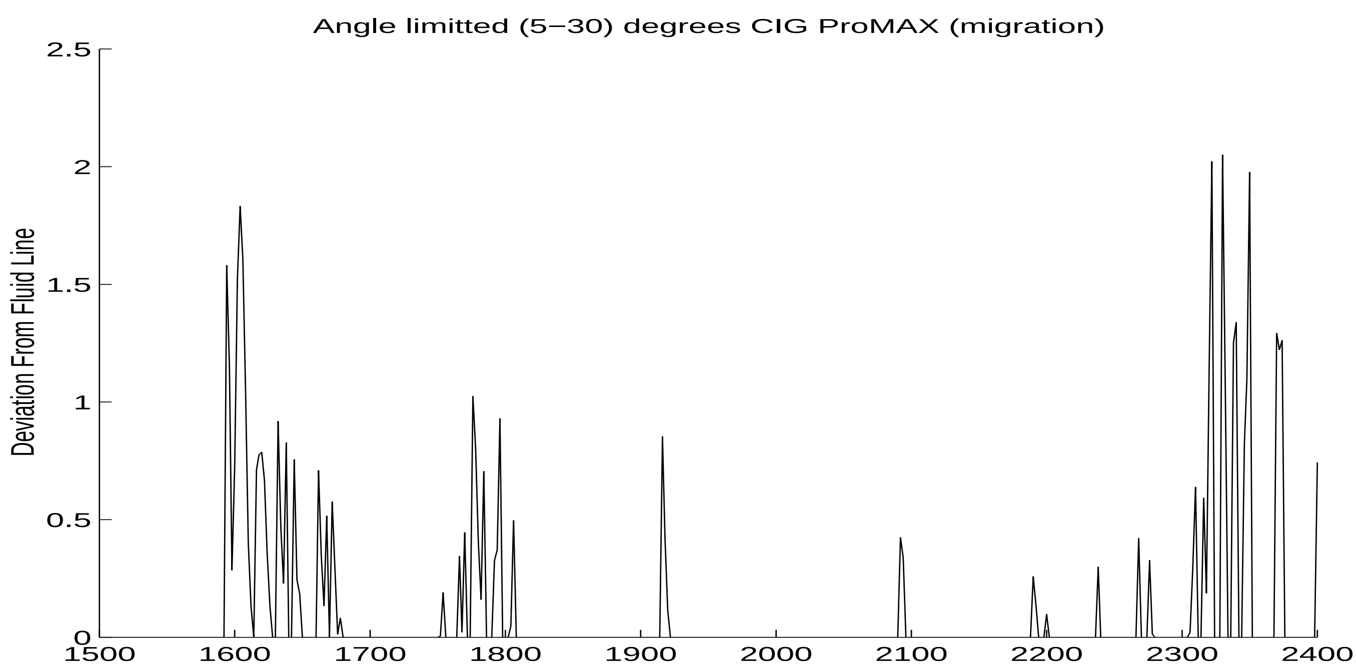

FIG. 23. Distance from fluid line, CIG from common-offset prestack Kirchhoff migration, spherical spreading correction applied to data before migration, wide aperture.

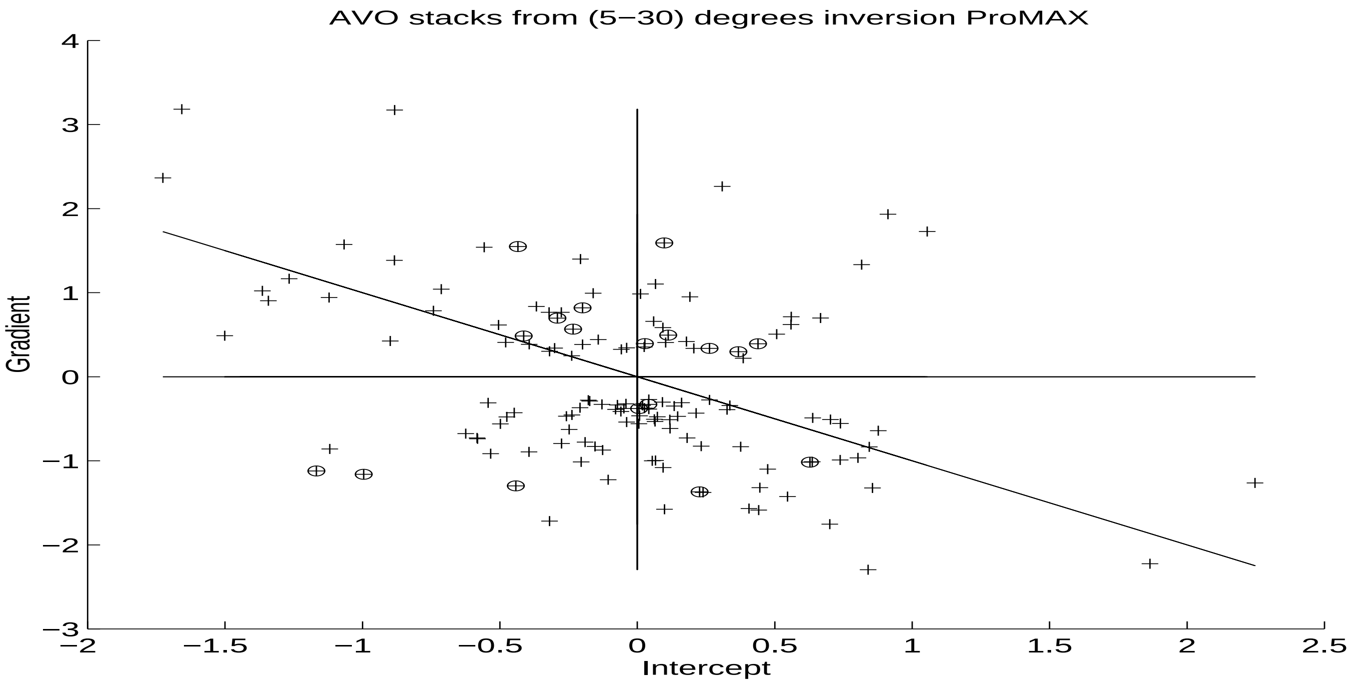

FIG. 24. Intercept versus gradient, CIG from common-offset 2D prestack Kirchhoff true amplitude migration, wide aperture.

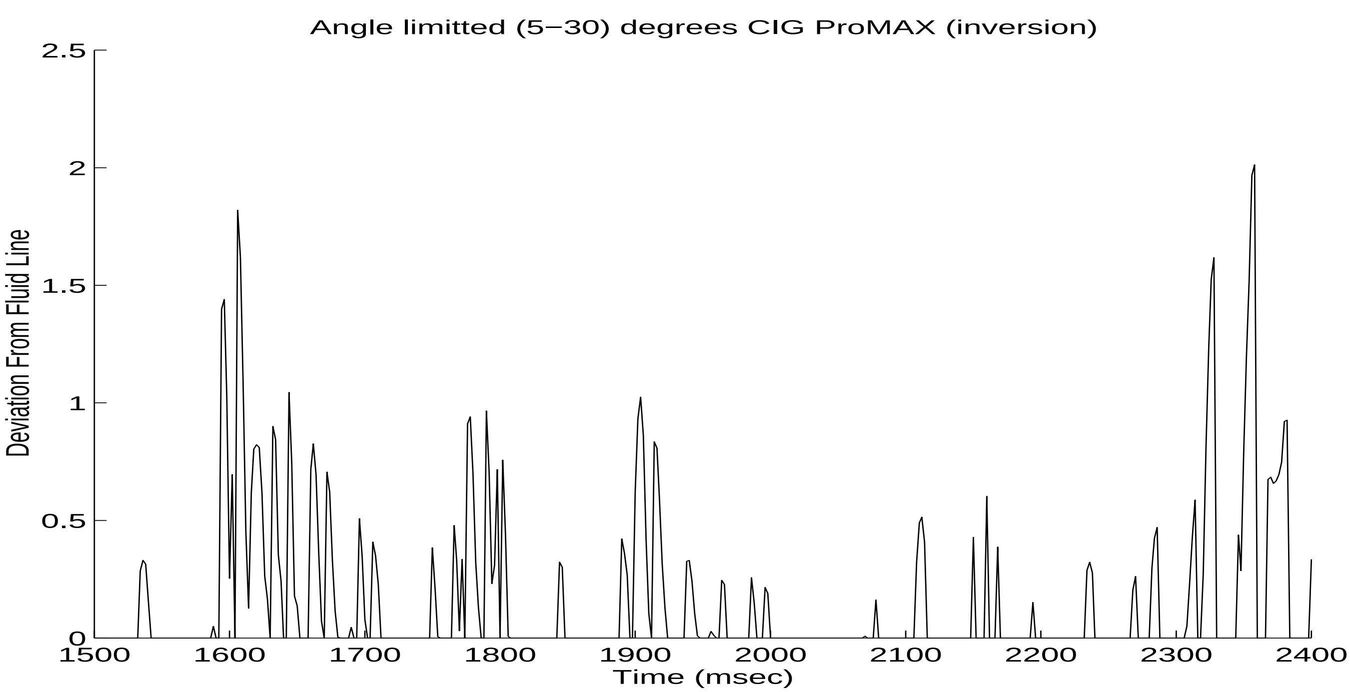

FIG. 25. Distance from fluid line, CIG from common-offset prestack Kirchhoff true amplitude migration, wide aperture.

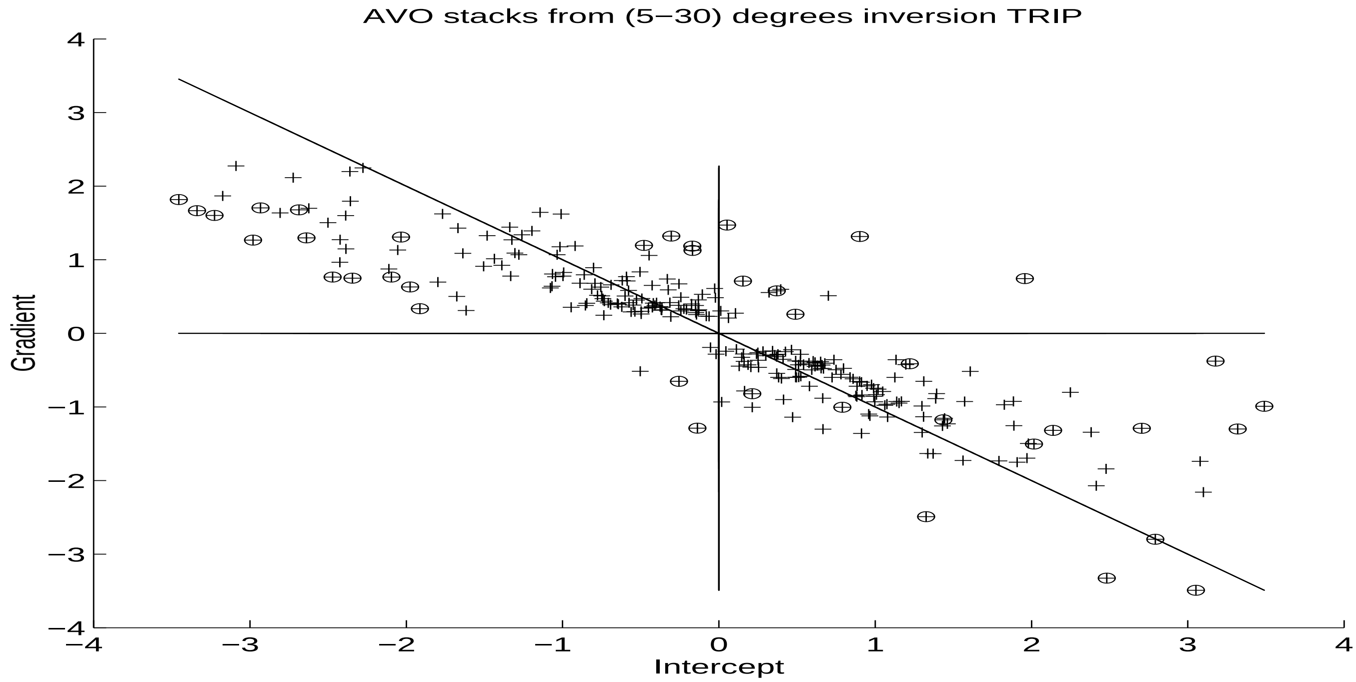

FIG. 26. Intercept versus gradient, CIG from asymptotic inversion, wide aperture.

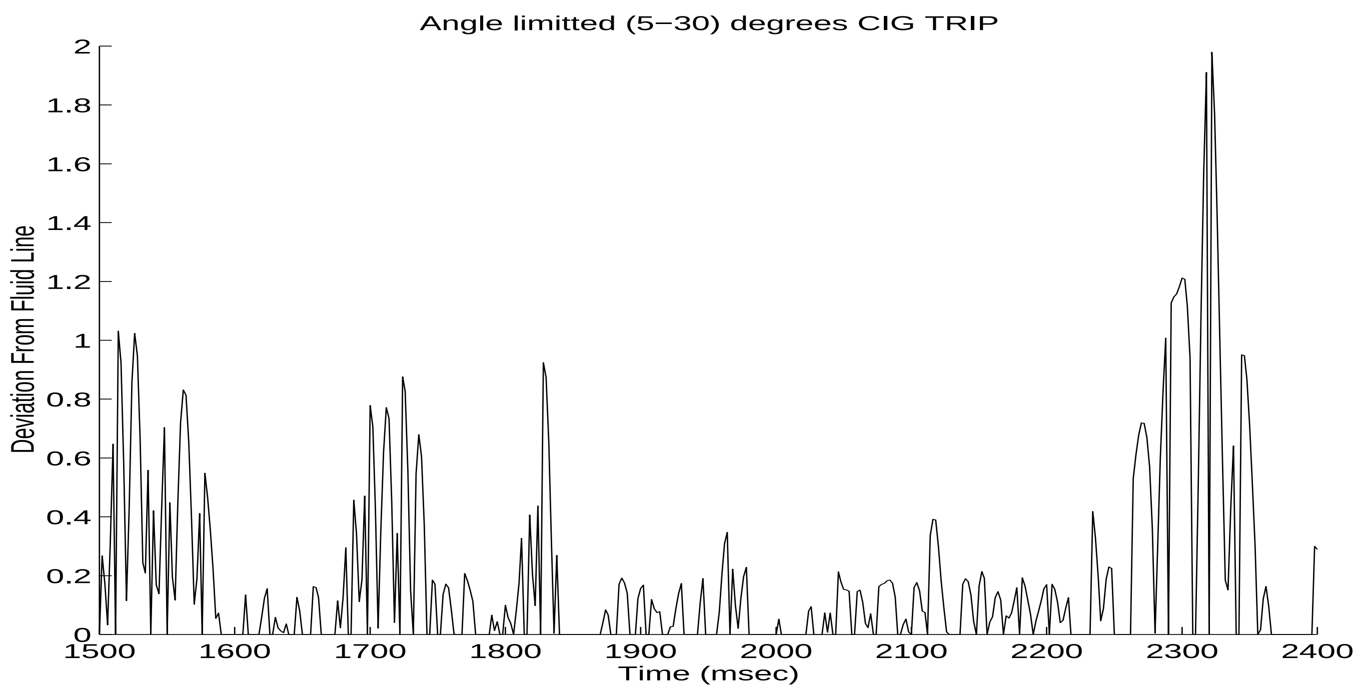

FIG. 27. Distance from fluid line, CIG from asymptotic inversion, wide aperture.

CONCLUSIONS

AVO processing of high quality marine data permitted us to examine the question: does amplitude processing affect the reliability of intercept and gradient estimates? We found that, amongst the alternatives we examined, only asymptotic inversion produced common image gather input to AVO attribute estimation which retained a key property, the clustering of shale and brine-sand data points around a fluid line, over the full range of angles permitted by Shuey's approximation to the Zoeppritz equations. While CDP based AVO also discriminated the very large gas sand in the study region from other parts of the sedimentary column, its discriminant power was considerably reduced by the large amount of scatter in the intercept vs. gradient crossplot.

The asymptotic inversion used in this work was based on the acoustic model (Araya and Symes, 1996). Since the reflectivity, even in Shuey's approximation, is based on linear elasticity, the use of the acoustic approximation requires some justification. We believe that the success of acoustic asymptotic inversion in this example is due to two somewhat accidental facts:

1. the background factors in the linearized Zoeppritz equation and its acoustic analogue differ by a slowly varying scale factor;

2. to second order in $\sin^2\theta$ both approximations have the same form though with different physical meanings for the coefficients.

Of course a treatment based directly on linearized elasticity would eliminate the need for such a conceptual stretch, (Bourgeois et al., 1989; Pan et al., 1993; Foster et al., 1997). The authors plan to explore this possibility in future work.

Acknowledgement and Disclaimer: This work was partially supported by the National Science Foundation under grant numbers DMS 9404283 and DMS 9627355; the Office of Naval Research under grant number N00014-96-1-0156; the Air Force Office of Scientific Research, Air Force Materials Command, USAF, under grant number F49620-95-1-0339; and The Rice Inversion Project. TRIP Sponsors for 1997 are Advance Geophysical, Amoco Production Co., Conoco Inc., Cray Research Inc., Discovery Bay, Exxon Production Research Co., Interactive Network Technologies, Mobil Research and Development Corp., and Shell International Research. The US Government is authorized to reproduce and distribute reprints for governmental purposes notwithstanding any copyright notation thereon. The views and conclusions contained herein are those of the authors and should not be interpreted as necessarily representing the official policies or endorsements, either expressed or implied, of the Air Force Office of Scientific Research, the Office of Naval Research, the National Science Foundation, or the US Government.

Special thanks are due to Dr. James J. Carazzone of Exxon Production Research Company for his invaluable advice and kind cooperation in supplying the field data from the Gulf of Mexico and Dr. Robert Baumel of Conoco, whose suggested this line of inquiry to us.

The seismic data processing in this paper was greatly facilitated by use of ProMAX™ 2D from Landmark Graphics.

REFERENCES

Araya, K. and Symes, W. W. (1996). 2D and 2.5D kirchhoff inversion using upwind finite difference amplitudes. In *Proc. 66th Annual International Meeting*, pages 503–506, Tulsa. Society of Exploration Geophysicists. Expanded abstract.

Bourgeois, A., Jiang, B., and Lailly, P. (1989). Linearized inversion: A significant step beyond pre-stack migration. *Geophysics J. Int.*, 99:435–445.

Foster, D. J., Keys, R. G., and Schmitt, D. P. (1997). Detecting subsurface hydrocarbons with elastic wavefields. In Chavent, G., Papanicolaou, G., Sacks, P., and Symes, W., editors, *Inverse Problems in Wave Propagation*. Springer Verlag, New York.

Pan, G., Young, C., and Castagna, J. (1993). Net pay delineation of gas sand using integrated target-oriented prestack elastic waveform inversion. In *63rd Annual International SEG Meeting*, pages 431–434, Washington, D.C., U.S.A. Society of Exploration Geophysicists. Expanded abstract.

Rutherford, S. R. and Williams, R. H. (1989). Amplitude-versus-offset variations in gas sands. *Geophysics*, 54:680–688.

Shuey, R. T. (1985). A simplification of zoeppritz equations. *Geophysics*, 50:609–614.

Smith, G. C. and Gidlow, P. M. (1987). Weighted stacking for rock property estimation and detection of gas. *Geophys. Prosp.*, 35:993–1014.

Spratt, S. (1987). Effect of normal moveout errors on amplitude versus offset-derived shear reflectivity. In *Proc. 57th Annual International Meeting*, pages 634–637, New Orleans. Society of Exploration Geophysicists. Expanded abstract.

Symes, W., Versteeg, R., Sei, A., and Tran, Q.-H. (1995a). Kirchhoff simulation, migration and inversion using finite difference traveltimes and amplitudes, Part I: Eikonal and transport solvers. Technical report, The Rice Inversion Project, Rice University, Houston, Texas, USA.

Symes, W., Versteeg, R., Sei, A., and Tran, Q.-H. (1995b). Kirchhoff simulation, migration and inversion using finite difference traveltimes and amplitudes, Part II: Modeling. Technical report, The Rice Inversion Project, Rice University, Houston, Texas, USA.